Identification of fluoxetine as a direct NLRP3 inhibitor to treat atrophic macular degeneration

Meenakshi Ambati[a,b,c,1], Ivana Apicella[a,b,1], Shao-bin Wang[a,b,1], Siddharth Narendran[a,b,d,1], Hannah Leung[a,b], Felipe Pereira[a,b,e], Yosuke Nagasaka[a,b], Peirong Huang[a,b], Akhil Varshney[a,b,2], Kirstie L. Baker[f], Kenneth M. Marion[f], Mehrdad Shadmehr[g], Cliff I. Stains[g,h], Brian C. Werner[i,3], Srinivas R. Sadda[f,j], Ethan W. Taylor[k], S. Scott Sutton[l], Joseph Magagnoli[l,3], and Bradley D. Gelfand[a,b,m,3]

aCenter for Advanced Vision Science, University of Virginia School of Medicine, Charlottesville, VA 22901; bDepartment of Ophthalmology, University of Virginia School of Medicine, Charlottesville, VA 22908; cCenter for Digital Image Evaluation, Charlottesville, VA 22901; dAravind Eye Hospital System, Madurai 625020, India; eDepartamento de Oftalmologia e Ciências Visuais, Escola Paulista de Medicina, Universidade Federal de São Paulo, São Paulo 04023-062, Brazil; fDoheny Eye Institute, Los Angeles, CA 90033; gDepartment of Chemistry, University of Virginia, Charlottesville, VA 22904; hUniversity of Virginia Cancer Center, University of Virginia, Charlottesville, VA 22908; iDepartment of Orthopaedic Surgery, University of Virginia School of Medicine, Charlottesville, VA 22908; jDepartment of Ophthalmology, David Geffen School of Medicine, University of California, Los Angeles, CA 90095; kDepartment of Chemistry and Biochemistry, University of North Carolina at Greensboro, Greensboro, NC 27412; lDepartment of Clinical Pharmacy and Outcomes Sciences, College of Pharmacy, University of South Carolina, Columbia, SC 29208; and mDepartment of Biomedical Engineering, University of Virginia School of Medicine, Charlottesville, VA 22908

The atrophic form of age-related macular degeneration (dry AMD) affects nearly 200 million people worldwide. There is no Food and Drug Administration (FDA)-approved therapy for this disease, which is the leading cause of irreversible blindness among people over 50 y of age. Vision loss in dry AMD results from degeneration of the retinal pigmented epithelium (RPE). RPE cell death is driven in part by accumulation of *Alu* RNAs, which are noncoding transcripts of a human retrotransposon. *Alu* RNA induces RPE degeneration by activating the NLRP3-ASC inflammasome. We report that fluoxetine, an FDA-approved drug for treating clinical depression, binds NLRP3 in silico, in vitro, and in vivo and inhibits activation of the NLRP3-ASC inflammasome and inflammatory cytokine release in RPE cells and macrophages, two critical cell types in dry AMD. We also demonstrate that fluoxetine, unlike several other antidepressant drugs, reduces *Alu* RNA–induced RPE degeneration in mice. Finally, by analyzing two health insurance databases comprising more than 100 million Americans, we report a reduced hazard of developing dry AMD among patients with depression who were treated with fluoxetine. Collectively, these studies identify fluoxetine as a potential drug-repurposing candidate for dry AMD.

fluoxetine | macular degeneration | retina | health insurance databases | molecular modeling

Age-related macular degeneration (AMD) is the leading cause of irreversible blindness among those over 50 y of age around the world (1). The dry form of AMD is characterized by degeneration of the retinal pigmented epithelium (RPE), a specialized monolayer of cells lying external to the retinal photoreceptors (2). Progressive RPE degeneration in the central portion of the retina known as the macula leads to photoreceptor cell death and consequent vision loss over several years (3). Dry AMD, which accounts for ~90% of the 200 million global cases of AMD (4), has no Food and Drug Administration (FDA)-approved therapy (5).

In dry AMD, areas of RPE degeneration display abnormal accumulation of *Alu* RNAs (6), which are noncoding RNAs transcribed from the highly abundant family of *Alu* repetitive elements in the human genome (7). These *Alu* RNAs as well as the related mouse retrotransposon B2 RNAs are cytotoxic (6, 8), as they activate the NLRP3-ASC inflammasome (9), a multiprotein complex that acts as a cellular danger sensor that responds to a diverse set of inflammatory stimuli (10, 11). In response to various danger signals, the proteins NLRP3 (nucleotide-binding domain, leucine-rich repeat receptor, and pyrin domain-containing protein 3), ASC (apoptosis-associated speck-like protein containing a caspase recruitment domain), and procaspase-1 assemble into a macromolecular

platform known as the ASC speck (12). The defining molecular event of inflammasome activation is autocleavage of procaspase-1 into active caspase-1. Active caspase-1, in turn, enzymatically cleaves two interleukins (ILs), IL-1β and IL-18, from their inactive proform to their mature, active forms. In dry AMD, activation of this inflammasome occurs both in RPE cells (9) and in macrophages (13) and leads to retinal cell death.

Despite dozens of clinical trials over two decades, no treatment has yet proven effective for dry AMD (5). We sought to identify

Significance

Dry age-related macular degeneration (AMD) affects the vision of millions of people worldwide. There is currently no Food and Drug Administration–approved treatment for dry AMD. The inflammasome components NLRP3 and ASC have been implicated in the pathogenesis of dry AMD. We report that fluoxetine, which is approved for the treatment of clinical depression, directly binds the NLRP3 protein and prevents NLRP3-ASC inflammasome assembly and activation. Fluoxetine prevents the degeneration of retinal pigmented epithelium cells in an animal model of dry AMD. We also present evidence from a big data analysis of health insurance databases that fluoxetine use is associated with reduced risk of developing dry AMD. These studies identify a potential repurposing candidate for a prevalent cause of blindness.

a therapy for dry AMD by employing the concept of drug repurposing (14). Specifically, we hypothesized that an existing drug that is FDA approved for another disease and that shares structural similarity to a known inflammasome inhibitor might be effective against dry AMD. In addition to testing its efficacy in preclinical models, we also sought to determine whether patients using this drug had a reduced hazard of developing dry AMD by analyzing health insurance claims databases. Therefore, we focused on a prevalent, chronic disease that has multiple treatment options: clinical depression.

Here, we provide evidence that fluoxetine, which is FDA approved for clinical depression, shares a structural moiety with the NLRP3 inhibitor CY-09 (15) and that fluoxetine interacts with NLRP3 and inhibits its assembly and activation. Furthermore, fluoxetine inhibits *Alu* RNA–induced RPE degeneration in mice. We also present evidence from two health insurance databases that fluoxetine use is associated with reduced incident dry AMD, suggesting that it potentially could be repurposed.

Results

Fluoxetine Interacts with NLRP3. The small molecule CY-09 is reported to bind to NLRP3 and inhibit inflammasome activation (15). By examining the structure of various FDA-approved drugs, we observed that fluoxetine, which is indicated for clinical depression, shared structural similarity to CY-09 in that both possessed a (trifluoromethyl)phenyl moiety (Fig. 1*A*).

To test whether fluoxetine binds NLRP3, we synthesized a biotin conjugate of fluoxetine. We then incubated biotinylated fluoxetine with protein lysate collected from lipopolysaccharide (LPS)-primed human THP-1 monocytes. Fluoxetine-associated protein complexes were precipitated by streptavidin pull down and found to contain NLRP3 by Western blotting, suggesting that fluoxetine exists in a complex with NLRP3 (Fig. 1*B*). In contrast, GAPDH was not detected in the same lysate pull down, indicating that fluoxetine did not nonspecifically bind random proteins in this assay (Fig. 1*B*). Next, a competition assay was performed by incubating the protein lysate and biotinylated fluoxetine with increasing amounts of excess unlabeled fluoxetine. Increasing ratios of unlabeled-to-labeled fluoxetine resulted in reduced abundance of NLRP3 detected in the precipitate (Fig. 1*B*). Ratios of 10-fold and higher excesses of

unlabeled fluoxetine resulted in undetectable levels of NLRP3. These data provide support for the specificity of the presumed interaction between fluoxetine and NLRP3.

Next, using an in vitro tube assay, we observed a direct interaction between biotinylated fluoxetine and recombinant GST-tagged NLRP3 protein (Fig. 1*C* and *SI Appendix*, Fig. S1). Excess amounts of unlabeled fluoxetine competed against this interaction, confirming the specificity of this interaction (Fig. 1*C*). Thus, similar to CY-09 (15), fluoxetine binds NLRP3. A previous study reported that CY-09 can bind to the ATP-binding domain of NLRP3 (15). To investigate whether fluoxetine binds NLRP3 in the same region as CY-09, we synthesized a biotin conjugate of CY-09 and incubated it with GST-NLRP3 and determined whether unlabeled fluoxetine competed with biotinylated CY-09. In agreement with earlier findings (15), we observed a direct interaction between biotinylated CY-09 and NLRP3 (Fig. 1*D*). In addition, we found that excess amounts of unlabeled fluoxetine competed against this interaction (Fig. 1*D*), which is compatible with the concept that fluoxetine interacts with the NLRP3 ATP-binding domain, where CY-09 is presumed to bind.

Since fluoxetine and CY-09 both contain a (trifluoromethyl)phenyl moiety, the above data suggest that this moiety could be relevant to their interaction with NLRP3. To further explore this possibility, we tested whether fluvoxamine, another small molecule that contains the same moiety (Fig. 1*A*), could disrupt fluoxetine's interaction with NLRP3. Indeed, excess amounts of unlabeled fluvoxamine competed against the interaction of biotinylated fluoxetine with NLRP3 in the protein lysates of LPS-primed human THP-1 monocyte (Fig. 1*E*). These data suggest that the (trifluoromethyl)phenyl moiety facilitates the interaction of these small molecules with the NLRP3 ATP-binding domain.

Fluoxetine Binds to the NLRP3 NACHT Domain In Silico with Predicted Submicromolar Affinity. Several lines of evidence point to structural mimicry of ATP, an essential ligand for NLRP3 activation, as a possible basis for the interaction of both CY-09 and fluoxetine with NLRP3. The trifluoromethyl (CF_3) group, which because of the strong electronegativity of fluorine, is an effective mimic for the terminal phosphate group of ATP. In addition, we have previously demonstrated that NLRP3 is inhibited by certain
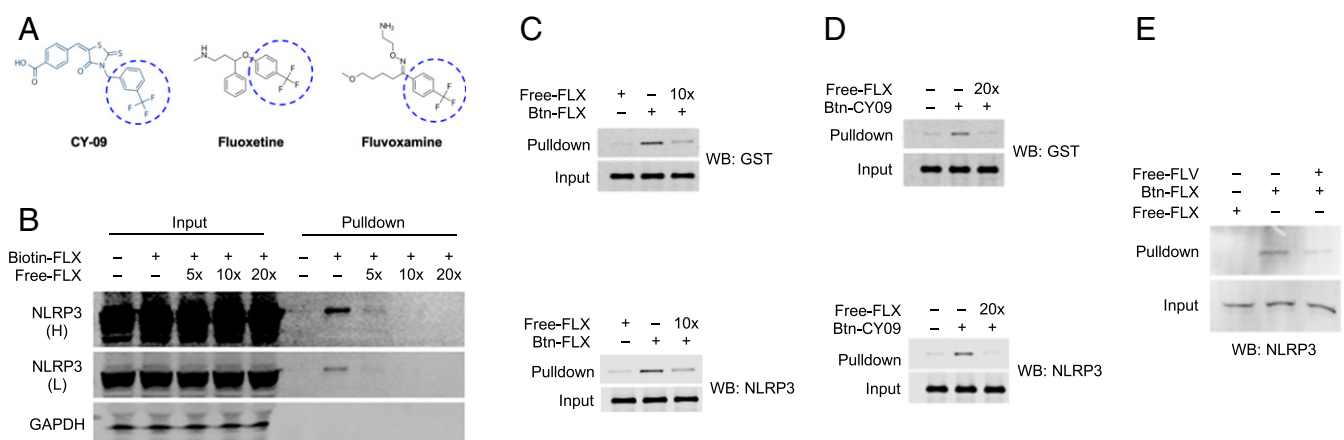

Fig. 1. In vitro binding analysis of fluoxetine with NLRP3. (*A*) CY-09, a small molecule inhibitor of NLRP3 (15), fluoxetine, and fluvoxamine all contain a (trifluoromethyl)phenyl moiety (highlighted in dashed circles). (*B*) Biotinylated fluoxetine was incubated with protein lysate collected from LPS-primed human THP-1 monocytes. Protein complexes were precipitated by streptavidin pull down. The input and pull-down fractions were immunoblotted for NLRP3 or GAPDH. Excess amounts of free (nonbiotinylated) fluoxetine were used as a competitor. Higher (H) and lower (L) exposures shown. (*C* and *D*) In vitro interaction of biotinylated fluoxetine (Btn-FLX, *C*) or biotinylated CY-09 (Btn-CY-09, *D*) with GST-NLRP3 protein analyzed by streptavidin pull down. The input and pull-down fractions were immunoblotted for GST (*Top*) and, for confirmation, NLRP3 (*Bottom*). Excess-free (nonbiotinylated) fluoxetine was used as a competitor. (*E*) Biotinylated fluoxetine was incubated with protein lysate collected from LPS-primed human THP-1 monocytes. Protein complexes were precipitated by streptavidin pull down. The input and pull-down fractions were immunoblotted for NLRP3. Excess-free (nonbiotinylated) fluvoxamine (FLV) was used as a competitor.

modified nucleoside analogs (16), which, as such, also have the potential to be inhibitors of ATP binding. Thus, we assessed the hypothesis that fluoxetine could be binding in the same structural region as ADP or ATP, a site that is deeply buried in the protein at the interface of several subdomains (NBD, WHD, and HD1) of the NACHT domain of NLRP3 as depicted in figure 2*A* of ref. 17.

We identified an unoccupied void in the ADP-binding cavity of NLRP3 in the 6NPY cryogenic electron microscopy (cryo-EM) structure (17) that is lined on one side by basic (positively charged) residues and can accommodate the entire triphosphate of ATP when it is projected into that void via a rotation around the nucleotide C4′−C5′ bond (Fig. 2 *A* and *B*). A modeled low-energy extended conformation of fluoxetine was docked in this cavity by superimposing the CF$_3$ of fluoxetine on the terminal phosphate group of ATP in this pose, with the second aromatic ring of the fluoxetine molecule overlapping the ATP ribose. This orients the *N*-methylamine sidechain of fluoxetine up toward the "exit" of the cavity, with a good preliminary steric fit of fluoxetine into the space (Fig. 2 *C* and *D*). Via a protein–ligand docking study using the HADDOCK web server (18), this mode of binding was confirmed as one of three clusters of docked poses in which fluoxetine was either wholly or partially inside the nucleotide-binding cavity. The pose shown in Fig. 2*E*, essentially identical to the manually docked pose of Fig. 2*C*, was the best ranked pose in the only cluster in which fluoxetine was fully inside the cavity. A schematic diagram of all of the interacting amino acid residues for this pose is shown in *SI Appendix*, Fig. S2*A*. In the two other clusters for docked fluoxetine, the fluoxetine molecule is essentially blocking the entrance to the nucleotide-binding cavity. The highest ranked is shown in Fig. 2*F*, with the fluoxetine amino group projecting out from the surface of the protein. The third cluster was similar but with the fluoxetine molecule inverted so that the CF$_3$ is projecting on the outside surface of the protein. However, these "partially inside" dockings may not be accessible in the actual NLRP3 molecule because there is an external loop of ~10 residues that is missing (disordered) in the 6NPY structure that is likely to partially occupy the region where fluoxetine is docked in these two clusters. So, the docking shown in Fig. 2*E* is overall the most relevant. The PRODIGY-LIGAND program (19, 20) was used to calculate the free energy of binding of fluoxetine to NLRP3, giving ΔG = −8.9 Kcal/mol, which corresponds to an inhibitory dissociation constant (K_i) of around 0.5 μM at 37 °C.

Fluoxetine Inhibits NLRP3 Assembly and Activation. We investigated whether fluoxetine disrupts inflammasome assembly, which we monitored by assessing ASC speck formation in mouse bone marrow–derived macrophages (BMDMs). ASC speck formation was robustly induced by *Alu* RNA transfection but decreased by fluoxetine treatment to baseline levels (Fig. 3 *A–D*). However, fluoxetine did not inhibit *NLRP3* messenger RNA expression (*SI Appendix*, Fig. S3), suggesting that it does not impair upstream inflammasome priming. Therefore, we assessed downstream inflammasome activation in BMDMs and immortalized human RPE cells (ARPE-19) by monitoring caspase-1 activation via Western blot analysis. Caspase-1 cleavage was robustly induced by *Alu* RNA or B2 RNA transfection in both BMDMs and ARPE-19 cells and reduced by fluoxetine treatment in both cell types (Fig. 3*E* and *SI Appendix,* Fig. S4).

Since fluoxetine targets NLRP3, we tested whether it inhibits inflammasome activation induced by other canonical NLRP3 activators such as ATP or nigericin in LPS-primed BMDMs (21–25). Indeed, we found that fluoxetine inhibited caspase-1 cleavage induced by ATP and IL-1β release induced by nigericin in these cells (*SI Appendix*, Fig. S5). Inflammasome activation was also assessed by quantifying IL-1β and IL-18 secretion in BMDMs and ARPE19 cells via enzyme-linked immunosorbent assay (ELISA). IL-1β and IL-18 release was induced by *Alu* RNA and B2 RNA in both

BMDMs and ARPE19 cells; this release was markedly reduced by fluoxetine treatment in both cell types (Fig. 3 *F–I*). These data demonstrate that fluoxetine inhibits a crucial output of inflammasome activation: inflammatory cytokine release.

Fluoxetine Inhibits RPE Degeneration. Next, the effects of fluoxetine and several other FDA-approved drugs belonging to various classes of antidepressants were tested in an in vivo mouse model of *Alu* RNA–induced RPE degeneration (6). RPE degeneration was assessed in two ways (26): 1) masked grading by two readers and 2) quantitative morphometric assessment of polymegethism—the variation in the size of RPE cells. *Alu* RNA induced RPE degeneration that resembled the morphology of RPE cells in human dry AMD, whereas intraocular delivery of fluoxetine conferred protection against RPE degeneration (Fig. 4*A*). In contrast, none of eight other antidepressants we tested were able to inhibit RPE degeneration (Fig. 4 *A* and *B*). None of the nine antidepressants tested induced RPE degeneration without *Alu* RNA treatment (*SI Appendix*, Fig. S6). We also found a dose-dependent effect of fluoxetine on inhibiting *Alu* RNA–induced RPE degeneration (*SI Appendix*, Fig. S7). These data reveal an inhibitory effect of fluoxetine in a human disease-relevant animal model and that fluoxetine exhibits a specific protective effect not possessed by multiple other FDA-approved antidepressants.

Fluoxetine Use Is Associated with Reduced Development of Dry AMD. The use of fluoxetine for the treatment of clinical depression for over 30 y afforded us the opportunity to assess the risk of development of dry AMD by performing a retrospective, longitudinal cohort analysis among patients aged 50 y or older (the population at risk for dry AMD development). We studied the Truven Marketscan Commercial Claims database, which contains data on 90 million Americans from 2006 to 2018, and the PearlDiver Mariner database, which contains data on 15 million Americans from 2010 to 2018 (*SI Appendix*, Tables S1 and S2).

We performed Kaplan–Meier survival analyses to estimate the probability of developing dry AMD: fluoxetine use was associated with a significantly slower rate of developing dry AMD in both the Truven and PearlDiver databases (Fig. 5 *A* and *B*). Next, we performed Cox proportional hazards regression analyses to estimate the hazard of dry AMD in relation to fluoxetine use. There were similar protective associations between fluoxetine exposure and incident dry AMD in the Truven (unadjusted hazard ratio, 0.705; 95% CI, 0.675 to 0.737; *P* < 0.001) and the PearlDiver databases (unadjusted hazard ratio, 0.704; 95% CI, 0.639 to 0.776; *P* < 0.001).

Patients in these databases were not randomly assigned to fluoxetine treatment; therefore, we performed propensity score matching, a causal inference approach used in observational studies (27–30), to assemble cohorts with similar baseline characteristics, thereby reducing possible bias in estimating treatment effects (*SI Appendix*, Tables S3 and S4). Additionally, to control for any residual covariate imbalance, we adjusted for confounders known to be associated with dry AMD: age, gender, smoking, and body mass index as well as Charlson comorbidity index, a measure of overall health. These adjusted Cox proportional hazards regression models in the propensity score–matched populations also revealed a protective association of fluoxetine use. In the Truven database, fluoxetine exposure was associated with a 9% reduced hazard of developing dry AMD (adjusted hazard ratio, 0.910; 95% CI, 0.854 to 0.968; *P* = 0.003). In the Mariner database, fluoxetine exposure was associated with a 22% reduced hazard of developing dry AMD (adjusted hazard ratio, 0.778; 95% CI, 0.685 to 0.885; *P* < 0.001).

Next, we estimated the combined hazard in the two databases based on an inverse variance–weighted meta-analysis using a random-effects model. We chose this model for two reasons: 1): a substantial amount of the variance between the studies could be attributed to heterogeneity (I^2 = 78.3%; 95% CI, 0.0 to 99.98%;
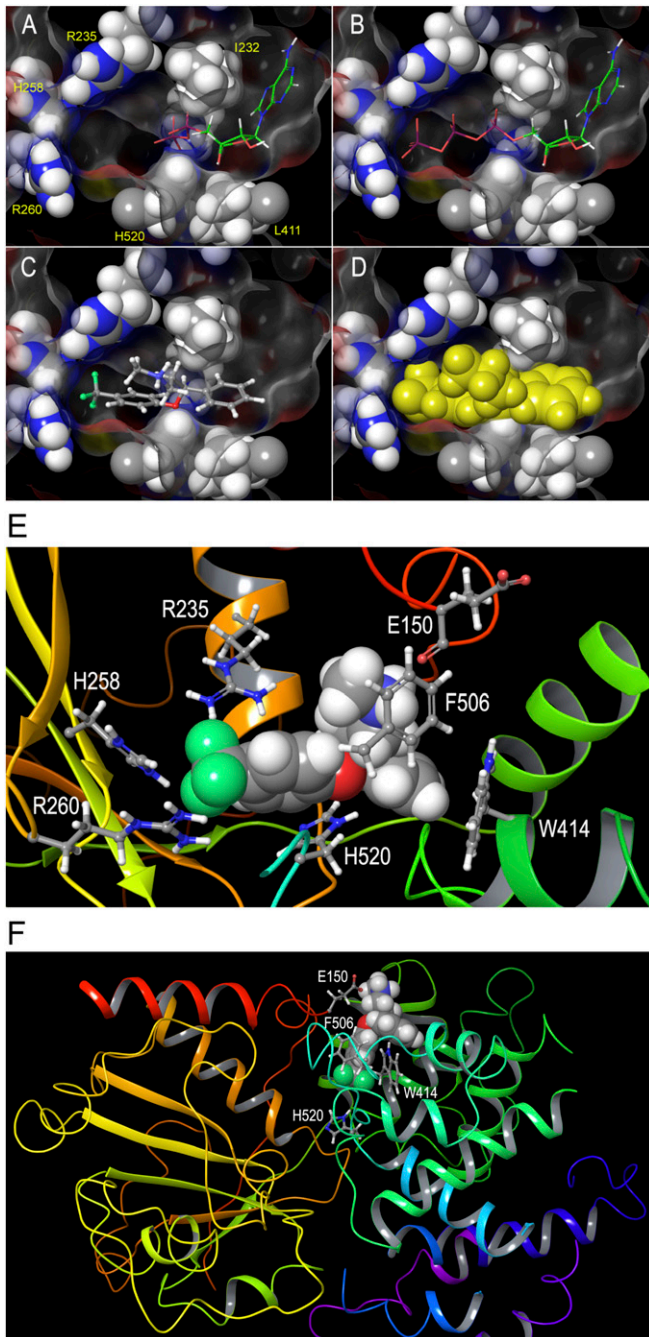
Ambati et al.
Identification of fluoxetine as a direct NLRP3 inhibitor to treat atrophic macular degeneration

PNAS | 3 of 9
https://doi.org/10.1073/pnas.2102975118

Fig. 2. In silico–binding analysis of fluoxetine with NLRP3. (*A–D*) Binding modes of ADP and ATP to NLRP3 as a basis for fluoxetine binding. (*A*) The fully internal cavity in which ADP is bound to the NACHT domain of NLRP3 is shown in a Z-clipped cutaway, with the internal protein surface and several key residues depicted, including several mostly hydrophobic residues that lead to a narrowing of the cavity around the nucleotide 5′ carbon (Ile232, Leu411. and His520) and a cluster of basic residues (Arg235, His258, and Arg260) at the left. In the 6NPY PDB structure shown, there is a substantial void in the cavity near those basic residues. (*B*) A simple rotation of the γ dihedral angle (C4′–C5′ bond) of the ribose sugar of the bound ADP to the -*sc* orientation, along with the addition of a terminal phosphate group to make ATP, shows that a bound ATP in an otherwise identical binding mode as ADP could engage in electrostatic interactions between the terminal phosphate oxygens and the triad of basic residues mentioned above, partially filling the void in the cavity. This could represent an alternate mode of ATP binding prior to hydrolysis, possibly associated with an inactive state. (*C*) The CF_3 group of fluoxetine, with negative charges on fluorine, could act as a phosphate isostere. If it is overlapped with the terminal phosphate group

$P = 0.03$), and 2) the Truven and PearlDiver databases represent populations whose underlying true effects are likely different (31–33). The random-effects meta-analysis identified a protective association of fluoxetine against incident dry AMD (pooled adjusted hazard ratio = 0.850; 95% CI, 0.730, 0.990; $P = 0.037$). For completeness, we also performed a meta-analysis using a fixed-effect model; this too revealed a similar fluoxetine protective association (Fig. 5*C*).

Discussion

Our studies provide evidence that fluoxetine directly binds NLRP3 and inhibits both NLRP3-ASC inflammasome assembly and activation. The docking results are compatible with the ability of the biotinylated fluoxetine analog to bind (shown experimentally in Fig. 1 *B* and *C*), as in the two best docked poses presented here (Fig. 2 *E* and *F*), the amino group to which the linker is attached at or nearest to the opening of the binding cavity, implying minimal disruption to the predicted mode of binding. The K_i of ~0.5 μM predicted by the docking simulations is compatible with the significant inhibition observed experimentally at a concentration of 10 μM. The circulating concentration of fluoxetine and its structurally similar bioactive metabolites in patients taking fluoxetine can reach 8 μM (34). This, combined with our finding that fluoxetine use in health insurance database analyses is associated with a reduced risk of developing dry AMD in people, supports the concept that oral administration of fluoxetine in humans can achieve levels capable of exerting biological activity against dry AMD. We also provide evidence that intraocular administration of fluoxetine prevents RPE degeneration in an animal model. As fluoxetine is a cell-permeable small molecule (35, 36), another potential mode of delivery is a sustained release intraocular implant, a drug delivery modality that has been used effectively for other ocular indications. Collectively, these findings provide a strong rationale for conducting a prospective randomized clinical trial of fluoxetine for dry AMD.

as modeled in *B*, a low-energy extended conformation of fluoxetine can be fitted onto the molecule of ATP shown in *B*, with the second aromatic ring of fluoxetine occupying the space of the ribose moiety. In this preliminary manual docking (see *Materials and Methods*), the *N*-methylamine sidechain of S-fluoxetine projects toward the viewer, that is, the part of the cavity closest to the protein surface. (*D*) This initial manual docking of S-fluoxetine into the nucleotide-binding cavity of NLRP3 is shown with the ligand in yellow space fill rendition, showing that S-fluoxetine has the potential to fit well within the experimentally observed cavity. This hypothesis was then assessed using in silico docking methods. (*E*) Best docked pose of S-fluoxetine fully inside the nucleotide-binding cavity as identified by HADDOCK. The conformation of the complex shown is after an OPLS3 force field minimization. The viewpoint is slightly rotated around the *y*-axis relative to *A* for clarity in showing the interacting side chains. These include the triad of basic residues mentioned in *A* (R235, H258, and R260, using the numbering system of 6NPY.PDB), two nitrogenous aromatic amino acids (H520 and W414), and two residues that engage the S-fluoxetine amino group in H-bonding (E150) or Pi-cation bonding (F506). The binding energy of this complex was calculated as ΔG = –8.9 Kcal/mol, using the PRODIGY-LIGAND web server (19, 20). A complete schematic interaction diagram for this complex is shown as *SI Appendix*, Fig. S2A. (*F*) Alternate docked pose of S-fluoxetine only partially inside the nucleotide-binding cavity. HADDOCK yielded a marginally slightly higher ranking to a cluster best represented by this complex in which S-fluoxetine interacts with four of the same residues as the "fully inside" complex shown in *E*. These residues include E150, except the fluoxetine amino group forms a salt bridge to the glutamate side chain rather than H-bonding to the backbone carbonyl. Trp414, Phe505, and His520 all interact with S-fluoxetine but in different ways. This conformation could represent an intermediate state of entry of fluoxetine into the buried cavity. The third least highly ranked cluster was similar to this, except the drug molecule is inverted with the CF_3 group of fluoxetine protruding slightly from the protein. It had less favorable electrostatic binding energy than the pose shown here with the amino group interacting with the glutamate side chain.
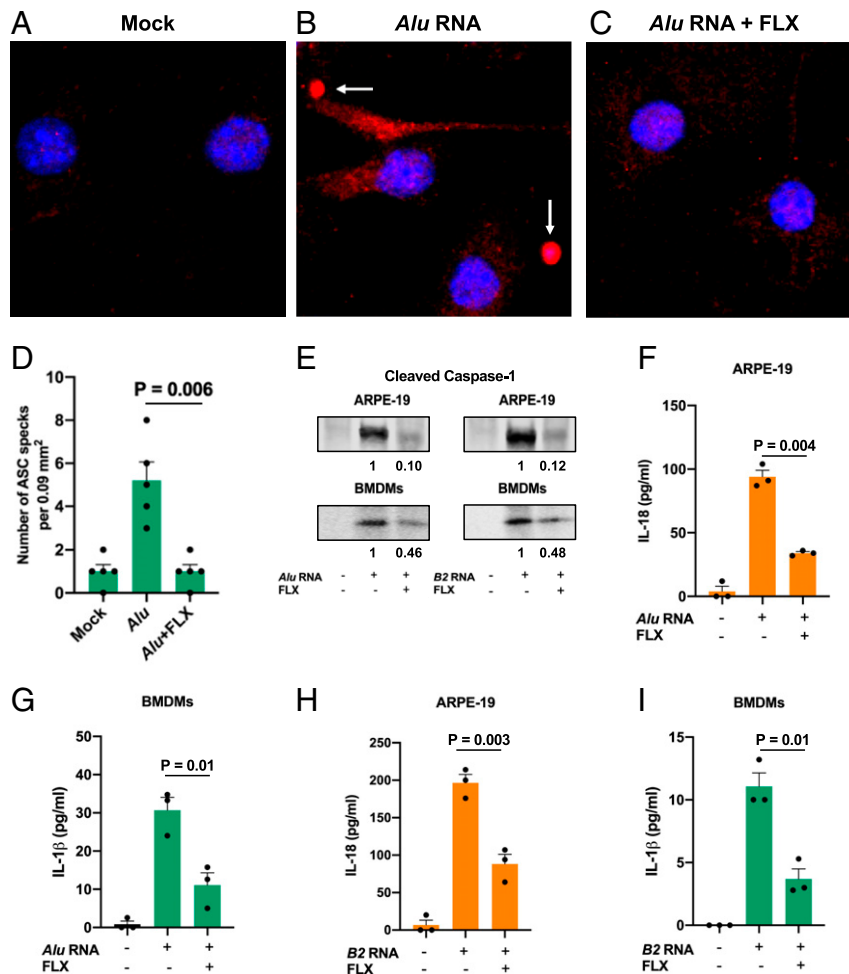
Fig. 3. Fluoxetine inhibits *Alu*/B2 RNA–induced NLRP3 inflammasome assembly and inflammasome activation. (*A–C*) Representative immunofluorescent images of ASC specks (red circles pointed to by white arrows) in wild-type mouse BMDMs that were mock transfected (*A*), transfected with *Alu* RNA (*B*), or transfected with *Alu* RNA and treated with fluoxetine (*C*). Cell nuclei stained blue by DAPI. (*D*) Bar graph of ASC speck quantification of *A* to *C*. $n = 5$ per group. (*E*) Representative Western blot images show that FLX inhibits caspase-1 cleavage induced by *Alu* RNA (*Left*) or B2 RNA (*Right*) in ARPE-19 cells (*Top*) and BMDMs (*Bottom*). Integrated densitometry values are shown below blots. $n = 3$ per group. (*F–I*) ELISA-based quantifications of cytokine release show that FLX inhibits IL-18 secretion by ARPE-19 cells (*F* and *H*) and IL-1β secretion by BMDMs (*G* and *I*) induced by *Alu* RNA (*F* and *G*) and B2 RNA (*H* and *I*). FLX, fluoxetine. $n = 3$ per group. All P values are for *Alu*/B2 RNA versus *Alu*/B2 RNA + FLX group comparisons using two-tailed Student's t test. Mean and SEM values are presented.

Despite numerous advances into the mechanisms of dry AMD, there is still no approved therapy for this disease. Traditional approaches to drug development can be expensive and time consuming: on average, a new FDA-approved drug takes 10 to 12 y and costs \$2.8 billion (present-day dollars) to develop (37). Our identification of the unrecognized therapeutic activity of an existing FDA-approved drug using big data mining, coupled with demonstrating its efficacy in a disease-relevant model, could greatly accelerate and reduce the cost of drug development. Indeed, we recently applied a similar strategy to identify an association between the use of nucleoside reverse transcriptase inhibitors (NRTIs) and a reduced risk of developing dry AMD (38). Given the toxicities of systemic NRTI use, fluoxetine or nontoxic NRTI derivatives known as Kamuvudines (16, 39) might be better candidates to evaluate in a prospective clinical trial.

A strength of our health insurance database analyses is that findings were replicated in two independent cohorts that comprise a substantial fraction of American adults with health insurance. In addition, we adjusted for confounders and performed propensity score matching, which increases the internal validity of our conclusion. However, because there was no randomization in our

study, residual confounding or selection bias might still exist. In addition, our study, like all observational health insurance claims studies, has inherent limitations in assessing the accuracy of coding and clinical phenotyping. Our studies do, however, provide a rationale for performing randomized controlled trials of fluoxetine for dry AMD, which can provide insights into causality. Demonstrating fluoxetine's benefit for dry AMD in such a prospective trial could benefit millions of patients suffering from the risk of irrecoverable blindness. It would also be interesting to determine whether fluoxetine is beneficial in other inflammasome-driven diseases such as Alzheimer's disease, Parkinson's disease, and diabetes (40, 41). Future studies could explore whether fluoxetine has additional targets, including other inflammasomes or inflammatory pathways, which could inform investigations into repurposing it for yet other diseases.

Materials and Methods

Synthesis of Biotinylated Fluoxetine. The reaction was performed in oven-dried glassware under N_2. All reagents and solvents were used as commercially supplied. High-performance liquid chromatography (HPLC) purification was performed using a Waters 1525 Binary HPLC pump with a 2489 ultraviolet/visible detector. Large-scale purification was done with a semi-prep column
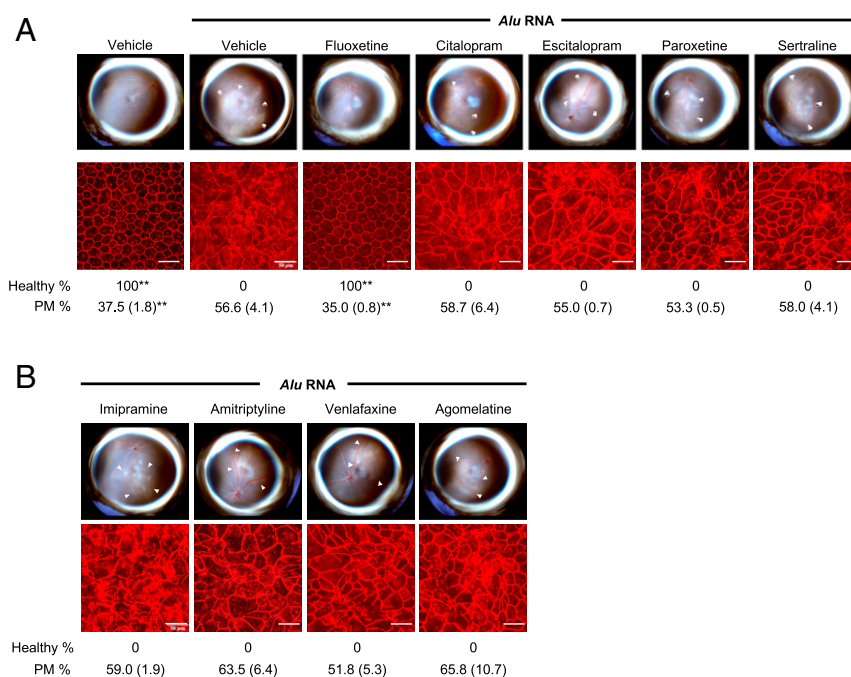
www.manaraa.com

MEDICAL SCIENCES

Fig. 4. *Alu* RNA–induced RPE degeneration is blocked by fluoxetine but not by other antidepressant drugs. (*A* and *B*) Subretinal administration of *Alu* RNA and intravitreous administration of selective serotonin reuptake inhibitor (SSRI) (*A*) and non-SSRI (*B*) antidepressant drugs in wild-type mice. (*Top*) Fundus photographs. (*Bottom*) Flat mounts stained for zonula occludens-1 (ZO-1; red). Degeneration outlined by white arrowheads. Binary (Healthy %) and morphometric (PM, polymegethism) (mean [SEM]) quantification of RPE degeneration is shown (Fisher's exact test for binary; two-tailed Student's *t* test for morphometry; **$P < 0.001$). Loss of regular hexagonal cellular boundaries in ZO-1–stained flat mounts is indicative of degenerated RPE. (Scale bars, 50 μm.)

(YMC-Pack ODS-A 5 μm, 250 × 20 mm) using a gradient of 10 to 95% acetonitrile containing 0.1% trifluoroacetic acid (TFA) over 47 mins in water containing 0.1% TFA. Mass spectrum was recorded using electrospray ionization (ESI) mass spectrometry (MS, Advion Expression, CMS, a single-quadrupole compact MS). Mass data are reported in units of *m/z* for [M+H]$^+$ or [M+Na]$^+$.
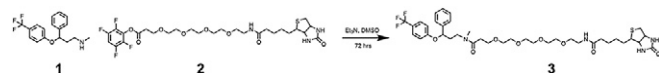
Fluoxetine (0.211 mmol, 65.5 mg, 4 equivalents, **1**) and TPF-PEG3-Biotin (0.052 mmol, 33.5 mg, 1 equivalent, **2**) were dissolved in dry dimethyl sulfoxide (DMSO; 2 mL) under a nitrogen atmosphere. An excess amount of triethylamine (0.1 mL, 13 eq) was added dropwise to the reaction vial. The reaction mixture was stirred vigorously under an inert atmosphere for 72 h followed by evaporation of the solvent and the remaining triethylamine under a high vacuum. The remaining colorless oil was dissolved in a mixture of acetonitrile and water (2 mL, 50/50 acetonitrile/water with 0.1% TFA) and purified by HPLC as described above. MS (ESI) *m/z* calculated for $C_{36}H_{53}F_3N_4O_6S$ [M+H]$^+$ = 783, found = 783 (biotinylated fluoxetine, 1 equivalent, **3**).

Synthesis of Biotinylated CY-09.
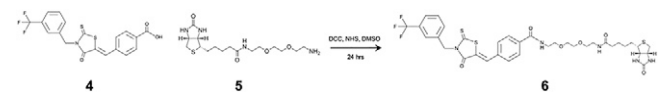
CY-09 (0.0236 mmol, 10 mg, 1 equivalent, **4**), Biotin-PEG2-Amine (0.0236 mmol, 8.9 mg, 1 equivalent, **5**), N,N′-dicyclohexylcarbodiimide (0.047 mmol, 11 mg, 2.1 eq), and N-Hydroxysuccinimide (0.047 mmol, 5.9 mg, 2 eq) were dissolved in dry DMSO (2 mL). The reaction mixture was stirred for 24 h at room temperature. The completion of reaction was monitored by thin-layer chromatography. The reaction mixture was dissolved in dichloromethane and washed with water and brine. The organic layer was dried with anhydrous $MgSO_4$, and the solvent evaporated. The product was purified by column chromatography using silica gel using methanol/dichloromethane as eluent. MS (ESI) *m/z* calculated for $C_{35}H_{40}F_3N_5O_6S_3$ [M+Na]$^+$ = 802, observed = 802 (biotinylated CY-09, 1 equivalent, **6**).

Streptavidin Pull-Down Assay. To assess the interaction of fluoxetine or CY-09 and NLRP3, LPS-primed THP-1 cell lysates or recombinant GST-tagged NLRP3 protein (H00114548-P01, Novus Biologicals) were precleared using streptavidin magnetic beads (88816, Thermo Fisher) to remove nonspecific binding. These pretreated proteins were incubated with biotinylated fluoxetine or biotinylated CY-09 and free (unbiotinylated) fluoxetine or free (unbiotinylated) fluvoxamine for 1 h on ice. Then, these samples were incubated with preactivated streptavidin magnetic beads overnight at 4 °C with rotation. On the next day, the beads were washed with lysis buffer three times and then boiled with sodium dodecyl sulfate (SDS) sample buffer (LC2676, Thermo Fisher) for further analysis.

Molecular Modeling and Docking of Fluoxetine–NLRP3 Complexes. The finding that fluoxetine inhibits inflammasome activation suggests that an appropriate template for the modeling of NLRP3 should be one in an inactive state rather than an activated state. Thus, we used the cryo-EM structure of ref. 17, Protein Data Bank (PDB) file 6NPY, as a template for modeling NLRP3 interactions with fluoxetine. As well as a bound ADP molecule, this structure features an NLRP3 monomer bound to NEK7, which was deleted from the structure prior to any additional modifications. The hook-shaped leucine-rich repeat domain to which NEK is predominantly bound was also deleted, leaving the NACHT domain, which has the nucleotide-binding domain near its center, with ADP bound in this structure (Fig. 2*A*). Fluoxetine was modeled using SybylX2.1 (Certara), and low-energy conformers were identified using systematic search, with seven rotatable bonds and electrostatics included. The distance D1 between the CF_3 carbon and *para*-H substituent on the unsubstituted phenyl ring was monitored, enabling identification of fully extended (highest D1) versus folded Y-shaped (lower D1) conformers. The global minimum had a low D1 and an internal H-bond between an amino NH and the ether oxygen but was too wide to fit in the nucleotide-binding cavity of NLRP3. A cluster of the lowest energy fully extended conformers was less than 1.5 Kcal/mol above the global minimum, easily attainable in an induced fit interaction. In binding to a protein, the internal H-bond is also likely to be disrupted by competing intermolecular H-bonding opportunities. Thus, the lowest energy extended conformation of fluoxetine was used to superimpose on the structure of ATP generated from the experimental ADP pose (as detailed in the legend to Fig. 2), with minor modifications to the methylamine side chain rotamers to minimize steric clashes in the cavity. Minimization of this all-atom complex using the OPLS3
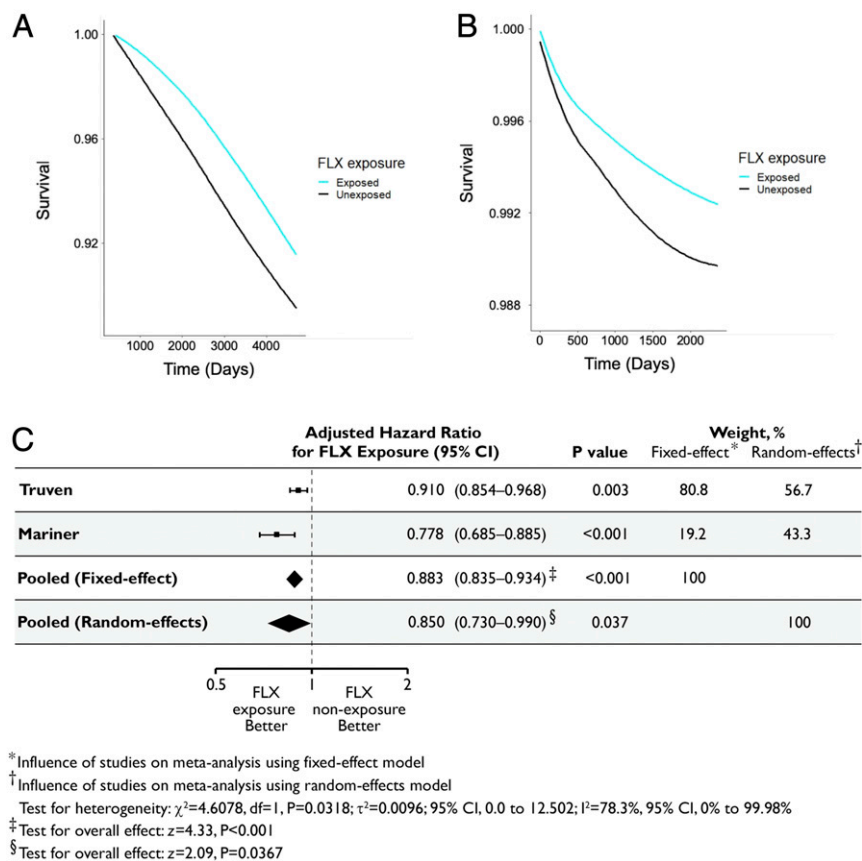
Fig. 5. Fluoxetine use is associated with reduced risk of developing dry AMD. (*A* and *B*) Kaplan–Meier survival curves showing the probability of not developing dry AMD (survival) over time for subjects in the Truven Marketscan (*A*) and PearlDiver Mariner (*B*) databases (baseline characteristics in *SI Appendix*, Tables S1 and S2) based on fluoxetine (FLX) exposure or nonexposure. Difference between FLX exposure or nonexposure groups was significant ($P < 0.0001$ by log-rank test). (*C*) HRs for developing dry AMD derived from propensity score–matched models (baseline characteristics in *SI Appendix*, Tables S3 and S4) adjusted for the confounding variables listed in *Methods and Materials* were estimated separately for the Truven Marketscan and PearlDiver Mariner databases. Adjusted HRs along with their 95% CIs are shown as black lines. Diamonds show the pooled estimate of the adjusted hazard ratio and the 95% CIs for meta-analyses using inverse variance–weighted random-effects and fixed-effect models. The broken vertical line represents an adjusted hazard ratio of 1, which denotes equal risk between FLX exposure and nonexposure. Horizontal bars denote 95% CIs. *P* values derived from z-statistics for individual databases are reported. The estimates of heterogeneity (χ^2), results of the statistical test of heterogeneity using the χ^2 test statistic and its degrees of freedom (df), and posterior probabilities of a nonbeneficial effect for each model are shown below the plot. The Higgins I^2 statistic and its 95% CI are presented. The results of the statistical tests of overall effect, the z-test statistics, and corresponding *P* values are presented.

force field as implemented in Maestro version 10.7 (Schrodinger, Inc.) generated the pose shown in Fig. 2 *C* and *D*. For this and subsequent docking calculations, several small gaps in the NLRP3 structure (disordered external loops) were not modeled but were capped with neutral amides, as these regions do not impinge on the core nucleotide-binding cavity, which is defined by residues highlighted in red in *SI Appendix*, Fig. S2*B*.

Using that definition of the binding region of interest, docking of the S enantiomer of fluoxetine in and around the nucleotide-binding cavity of the truncated NLRP3 structure was performed using the HADDOCK2.4 web server at the University of Utrecht van Zundert et al. (18). HADDOCK successfully identified three clusters of poses for S-fluoxetine interacting with at least some residues within the nucleotide-binding cavity. The "best" conformer in one of those three clusters was essentially identical to the pose identified by the ligand overlap approach (Fig. 2). The PRODIGY-LIGAND program from the same research group (19, 20) was used to calculate the free energy of the binding of fluoxetine to NLRP3 from the HADDOCK output PDB file of the docked complex.

Cell Culture Studies. All cell culture experiments were compliant with the University of Virginia Institutional Biosafety Committee regulations. The human retinal pigment epithelial cell line ARPE-19 (American Type Culture Collection) was maintained in Dulbecco's Modified Eagle Medium supplemented with 10% fetal bovine serum (FBS) and standard antibiotics. Mouse BMDMs were cultured in Iscove's modified Dulbecco's media with 10% FBS

and 20% L929 supernatants. All cells were maintained at 37 °C in a 5% CO_2 environment.

ASC speck imaging. BMDMs seeded on chambered coverslips (30,000 cells/well) for 12 h were pretreated with fluoxetine (10 μM) or 0.1% DMSO (control) for 2 h. Cells were transfected with *Alu* RNA using Lipofectamine 3000 (Thermo Fisher) for 12 h. Coverslips were fixed with 2% paraformaldehyde (15 min at room temperature), washed with phosphate-buffered saline (PBS), permeabilized, blocked with blocking buffer (PBS, 0.1% TX-100, 5% normal goat serum; 1 h at 4 °C), incubated with anti-ASC antibody (Adipogen; 1:300) with blocking buffer, and visualized with Alexa Fluor 555 (Invitrogen). Nuclei were stained with DAPI. Slides mounted using Fluoromount-G (SouthernBiotech) were imaged by confocal microscopy (Nikon A1R). The number of specks per 0.09 mm^2 field among the mock-transfected, *Alu*-transfected, and *Alu*-transfected and fluoxetine-treated cells were compared by two-tailed Student's *t* test. Mean and SEM values are presented.

Immunoblotting. Cells were transfected with *Alu* RNA or *B2* RNA or mock transfected for 12 h (BMDMs) and 48 h (ARPE-19). BMDMs were stimulated with LPS (125 ng/mL) for 4 h and ATP (5 mM) for 30 min. For all experiments, cells were pretreated with fluoxetine (10 μM) for 1 h and again after transfection or activating stimulus. Proteins from the cell-free supernatant were precipitated by adding sodium deoxycholate (0.15% final) followed by adding trichloroacetic acid (TCA) (7.2% final) and incubating on ice overnight. Samples were spun down at 13,000 × *g* for 30 min, and pellets were washed two times with ice-cold acetone. Precipitated proteins solubilized in 4× lithium dodecyl sulfate Buffer with 2-mercaptoethanol were resolved by SDS-polyacrylamide

Ambati et al.
Identification of fluoxetine as a direct NLRP3 inhibitor to treat atrophic macular degeneration

www.manaraa.com

gel electrophoresis on Novex Tris-Glycine Gels (Invitrogen) and transferred onto Immobilon-FL polyvinylidene fluoride membranes (Millipore). The transferred membranes were blocked with Odyssey Blocking Buffer (PBS) for 1 h at room temperature and then incubated with primary antibody at 4 °C overnight. The immunoreactive bands were visualized using species-specific secondary antibodies conjugated with IRDye. Blot images were captured using an Odyssey imaging system. The antibodies used were as follows: mouse monoclonal anti-human caspase-1 antibody (AdipoGen; 1:1,000) and mouse monoclonal anti-mouse caspase-1 antibody (AdipoGen; 1:1,000). Expression levels are presented as integrated densitometry values (ImageJ, NIH).

IL-1β and IL-18 ELISA. BMDMs and ARPE-19 cells were transfected with *Alu* RNA or *B2* RNA or mock transfected and treated with fluoxetine (10 μM) as above. BMDMs were pretreated with various doses of fluoxetine for 1 h and then primed with LPS (125 ng/mL) for 4 h and exposed to nigericin, sodium salt (InvivoGen, 20 μM) overnight. Secreted mouse IL-β and human IL-18 in the conditioned cell culture media were detected using ELISA kits (R&D Systems) according to the manufacturer's instructions. Mean and SEM values are presented. Groups were compared by two-tailed Student's *t* test or, for multidose experiments, one-way ANOVA with Dunnett's multiple comparisons test.

Real-time PCR. ARPE-19 cells were transfected with *B2* RNA or mock transfected for 4 h and pretreated with fluoxetine (10 μM) for 1 h and again after *B2* RNA transfection. RNA was extracted from cells using TRIZOL reagent (Invitrogen) following the manufacturer's instructions, DNase treated, and reverse transcribed (QuantiTect, QIAGEN). The reverse transcribed (RT) products (complementary DNA) were amplified by real-time PCR (qPCR) (Applied Biosystems) with Power SYBR Green Master Mix (Thermo Fisher). The qPCR cycling conditions were 50 °C for 2 min and 95 °C for 10 min followed by 40 cycles of a two-step amplification program (95 °C for 15 s and 58 °C for 1 min). Relative expression of target genes was determined by the $2^{-\Delta\Delta Ct}$ method. For negative controls, no RT products were used as templates in the qPCR. Primers used in this assay were as follows: human NLRP3 forward 5′-TAATCAGAATCT-CACGCACCT-3′ and reverse 5′-TTCACAGAACATCATGACCCC-3′, and human GAPDH forward 5′-AGCCTCAAGATCATCAGCAATG-3′ and reverse 5′-ATGGAC-TGTGGTCATGAGTCCTT-3′.

Animal Studies. Animal experiments were approved by the University of Virginia Institutional Animal Care and Use Committee. C57BL/6J mice (The Jackson Laboratory) were anesthetized with ketamine hydrochloride and xylazine.

Induction of RPE degeneration and drug treatments. In vitro–transcribed *Alu* RNA (300 ng in 1 μL) or vehicle control (PBS) were injected subretinally. Fluoxetine, citalopram, paroxetine, sertraline, escitalopram, venlafaxine, amitriptyline, imipramine, agomelatine (all from Cayman Chemical; 1 mM in 0.5 μL), or PBS was injected into the vitreous humor 24 h before and immediately after *Alu* RNA injections. A dose-ranging experiment using fluoxetine was also performed. Animals were euthanized 7 d after *Alu* RNA injection, and the eyes were enucleated.

Assessment of RPE degeneration. RPE health was assessed by immunofluorescence staining of zonula occludens-1 (ZO-1) on RPE flat mounts. Flat mounts were fixed with 2% paraformaldehyde, stained with rabbit polyclonal antibodies against mouse ZO-1 (Invitrogen; 1:100), visualized with Alexa Fluor 594 (Invitrogen), and imaged (A1R Nikon confocal microscope). Images were graded as healthy or degenerated in masked fashion. Proportions of eyes with degeneration among the various antidepressant treatment groups were compared using Fisher's exact test. Polymegethism quantified by morphometry was compared using two-tailed Student's *t* test. For the dose-ranging experiment, the Cochran–Armitage trend test was used to test whether the proportions of eyes with degeneration varied linearly with fluoxetine dose. To test for trends in polymegethism values in the dose-ranging experiment, we used a simple regression analysis with polymegethism as the dependent variable and the dosage as the independent variable. Dosage was entered into the model with a linear effect, and the regression model was estimated using ordinary least squares. Robust SEs were utilized to account for heteroscedasticity in the residuals.

Health Insurance Claims Database Analysis.
Data source. We used claims data from the Truven MarketScan Commercial Claims database (IBM), containing health care claims and medication usage from the commercial insurance claims from employer-based health insurance beneficiaries from 2006 to 2018, and from the PearlDiver Mariner database, which contains data on health care claims and medication usage for persons in provider networks over the time period 2010 to the second quarter of 2018. These data are Health Insurance Portability and Accountability Act compliant and were deemed by the University of Virginia Institutional Review Board (IRB) as exempt from IRB approval requirements.
Sample selection. Patients were included in the analysis if they had continuous enrollment in the plan for at least 1 y and were at least 50 y of age at baseline. Individuals with preexisting dry AMD (one or more medical claims prior to diagnosis of depression) were excluded. Disease claims were identified by International Classification of Diseases (ICD)-9-CM and ICD-10-CM codes.
Independent variable. Exposure to fluoxetine—the independent variable—was determined by whether patients filled ≥1 outpatient pharmacy prescriptions for generic or brand versions, either in sole form or as a combination medication, as identified by National Drug Codes.
Dependent variable. The time to initial diagnosis of dry AMD was the dependent variable for this analysis.
Analyses. To analyze the risk of dry AMD between fluoxetine users and fluoxetine nonusers, Kaplan–Meier survival plots were generated and analyzed by the log-rank test. To reduce residual confounding, we utilized propensity score methods. The individual propensities for starting fluoxetine treatment were estimated via logistic regression and use demographics and comorbid conditions as predictors. The logit of the propensity score was used to form 1:1 ratio matches via the greedy nearest neighbor algorithm. In addition, to control for any residual covariate imbalance, we estimated the hazard ratio with the propensity score–matched data using the multivariable Cox models. Matching variables including age, gender, smoking, body mass index, and Charlson comorbidity index were included to provide doubly robust estimates. Statistical tests were two-sided. *P* values < 0.05 were considered statistically significant. Analyses were performed with the use of R software, version 3.6.1 (the R project [https://www.r-project.org]) and SAS 9.4 (SAS Institute, Inc.).
Meta-analysis. An inverse variance–weighted meta-analysis of the two databases was performed to estimate the combined hazard ratio (HR) and to compute 95% CIs using a random-effects model. Meta-analysis was performed using the R package metafor. The restricted maximum likelihood estimator was used to estimate the between-study variance (τ^2). The variability between the two databases was assessed using Cochran's Q-test. A forest plot was generated to display the HR and 95% CI of each study and of the pooled results.

Data Availability. All data needed to evaluate the conclusions in this paper are available in the main text and *SI Appendix*.

1. J. Ambati, B. K. Ambati, S. H. Yoo, S. Ianchulev, A. P. Adamis, Age-related macular degeneration: Etiology, pathogenesis, and therapeutic strategies. *Surv. Ophthalmol.* **48**, 257–293 (2003).
2. J. Ambati, B. J. Fowler, Mechanisms of age-related macular degeneration. *Neuron* **75**, 26–39 (2012).
3. L. L. Shen, M. Sun, S. Khetpal, H. K. Grossetta Nardini, L. V. Del Priore, Topographic variation of the growth rate of geographic atrophy in nonexudative age-related macular degeneration: A systematic review and meta-analysis. *Invest. Ophthalmol. Vis. Sci.* **61**, 2 (2020).
4. W. L. Wong *et al.*, Global prevalence of age-related macular degeneration and disease burden projection for 2020 and 2040: A systematic review and meta-analysis. *Lancet Glob. Health* **2**, e106–e116 (2014).
5. P. Mitchell, G. Liew, B. Gopinath, T. Y. Wong, Age-related macular degeneration. *Lancet* **392**, 1147–1159 (2018).
6. H. Kaneko *et al.*, DICER1 deficit induces Alu RNA toxicity in age-related macular degeneration. *Nature* **471**, 325–330 (2011).
7. H. H. Kazazian Jr, J. V. Moran, Mobile DNA in health and disease. *N. Engl. J. Med.* **377**, 361–370 (2017).

8 of 9 | **PNAS**
https://doi.org/10.1073/pnas.2102975118

Ambati et al.
Identification of fluoxetine as a direct NLRP3 inhibitor to treat atrophic macular degeneration

8. S. Dridi et al., ERK1/2 activation is a therapeutic target in age-related macular degeneration. Proc. Natl. Acad. Sci. U.S.A. 109, 13781–13786 (2012).

9. V. Tarallo et al., DICER1 loss and Alu RNA induce age-related macular degeneration via the NLRP3 inflammasome and MyD88. Cell 149, 847–859 (2012).

10. E. Latz, The inflammasomes: Mechanisms of activation and function. Curr. Opin. Immunol. 22, 28–33 (2010).

11. J. Ambati, J. P. Atkinson, B. D. Gelfand, Immunology of age-related macular degeneration. Nat. Rev. Immunol. 13, 438–451 (2013).

12. J. Masumoto et al., ASC, A novel 22-kDa protein, aggregates during apoptosis of human promyelocytic leukemia HL-60 cells. J. Biol. Chem. 274, 33835–33838 (1999).

13. C. M. Eandi et al., Subretinal mononuclear phagocytes induce cone segment loss via IL-1β. eLife 5, e16490 (2016).

14. M. S. Boguski, K. D. Mandl, V. P. Sukhatme, Drug discovery. Repurposing with a difference. Science 324, 1394–1395 (2009).

15. H. Jiang et al., Identification of a selective and direct NLRP3 inhibitor to treat inflammatory disorders. J. Exp. Med. 214, 3219–3238 (2017).

16. B. J. Fowler et al., Nucleoside reverse transcriptase inhibitors possess intrinsic anti-inflammatory activity. Science 346, 1000–1003 (2014).

17. H. Sharif et al., Structural mechanism for NEK7-licensed activation of NLRP3 inflammasome. Nature 570, 338–343 (2019).

18. G. C. P. van Zundert et al., The HADDOCK2.2 web server: User-friendly integrative modeling of biomolecular complexes. J. Mol. Biol. 428, 720–725 (2016).

19. Z. Kurkcuoglu et al., Performance of HADDOCK and a simple contact-based protein-ligand binding affinity predictor in the D3R Grand Challenge 2. J. Comput. Aided Mol. Des. 32, 175–185 (2018).

20. A. Vangone et al., Large-scale prediction of binding affinity in protein-small ligand complexes: The PRODIGY-LIG web server. Bioinformatics 35, 1585–1587 (2019).

21. T. D. Kanneganti et al., Bacterial RNA and small antiviral compounds activate caspase-1 through cryopyrin/Nalp3. Nature 440, 233–236 (2006).

22. S. Mariathasan et al., Cryopyrin activates the inflammasome in response to toxins and ATP. Nature 440, 228–232 (2006).

23. F. Martinon, V. Pétrilli, A. Mayor, A. Tardivel, J. Tschopp, Gout-associated uric acid crystals activate the NALP3 inflammasome. Nature 440, 237–241 (2006).

24. R. Muñoz-Planillo et al., K⁺ efflux is the common trigger of NLRP3 inflammasome activation by bacterial toxins and particulate matter. Immunity 38, 1142–1153 (2013).

25. F. S. Sutterwala et al., Critical role for NALP3/CIAS1/Cryopyrin in innate and adaptive immunity through its regulation of caspase-1. Immunity 24, 317–327 (2006).

26. N. Kerur et al., cGAS drives noncanonical-inflammasome activation in age-related macular degeneration. Nat. Med. 24, 50–61 (2018).

27. P. R. Rosenbaum, D. B. Rubin, The central role of the propensity score in observational studies for causal effects. Biometrika 70, 41–55 (1983).

28. K. Imai, D. A. van Dyk, Causal inference with general treatment regimes. J. Am. Stat. Assoc. 99, 854–866 (2004).

29. J. S. Haukoos, R. J. Lewis, The propensity score. JAMA 314, 1637–1638 (2015).

30. H. Ohlsson, K. S. Kendler, Applying causal inference methods in psychiatric epidemiology: A review. JAMA Psychiatry 77, 637–644 (2020).

31. R. DerSimonian, N. Laird, Meta-analysis in clinical trials. Control. Clin. Trials 7, 177–188 (1986).

32. C. Anello, J. L. Fleiss, Exploratory or analytic meta-analysis: Should we distinguish between them? J. Clin. Epidemiol. 48, 109–116, discussion 117–118 (1995).

33. J. Lau, J. P. Ioannidis, C. H. Schmid, Summing up evidence: One answer is not always enough. Lancet 351, 123–127 (1998).

34. S. H. Preskorn, B. Silkey, J. Beber, C. Dorey, Antidepressant response and plasma concentrations of fluoxetine. Ann. Clin. Psychiatry 3, 147–151 (1991).

35. J. Mukherjee, M. K. Das, Z. Y. Yang, R. Lew, Evaluation of the binding of the radio-labeled antidepressant drug, 18F-fluoxetine in the rodent brain: An in vitro and in vivo study. Nucl. Med. Biol. 25, 605–610 (1998).

36. W. A. Daniel, J. Wójcikowski, A. Pałucha, Intracellular distribution of psychotropic drugs in the grey and white matter of the brain: the role of lysosomal trapping. Br. J. Pharmacol. 134, 807–814 (2001).

37. J. A. DiMasi, H. G. Grabowski, R. W. Hansen, Innovation in the pharmaceutical industry: New estimates of R&D costs. J. Health Econ. 47, 20–33 (2016).

38. S. Fukuda et al., Cytoplasmic synthesis of endogenous Alu complementary DNA via reverse transcription and implications in age-related macular degeneration. Proc. Natl. Acad. Sci. U.S.A. 118, e2022751118 (2021).

39. S. Narendran et al., Nucleoside reverse transcriptase inhibitors and Kamuvudines inhibit amyloid-β induced retinal pigmented epithelium degeneration. Signal Transduct. Target. Ther. 6, 1–9 (2021).

40. M. T. Heneka, R. M. McManus, E. Latz, Inflammasome signalling in brain function and neurodegenerative disease. Nat. Rev. Neurosci. 19, 610–621 (2018).

41. S. L. Masters, E. Latz, L. A. O'Neill, The inflammasome in atherosclerosis and type 2 diabetes. Sci. Transl. Med. 3, 81ps17 (2011).

MEDICAL SCIENCES

www.manaraa.com